Optics Letters

Photonic crystal fiber interferometric vector bending sensor

JOEL VILLATORO,[1,2,*] VLADIMIR P. MINKOVICH,[1,3] AND JOSEBA ZUBIA[1]

[1]Department of Communications Engineering, Escuela Técnica Superior de Ingeniería (ETSI) de Bilbao, University of the Basque Country (UPV/EHU), Alda. Urquijo s/n, E-48013 Bilbao, Spain
[2]IKERBASQUE—Basque Foundation for Science, E-48011 Bilbao, Spain
[3]Centro de Investigaciones en Optica A. C., 37150, Leon, GTO, Mexico
*Corresponding author: agustinjoel.villatoro@ehu.es

Received 15 April 2015; revised 29 May 2015; accepted 9 June 2015; posted 10 June 2015 (Doc. ID 238128); published 26 June 2015

A compact and highly sensitive interferometric bending sensor (inclinometer) capable of distinguishing the bending or inclination orientation is demonstrated. The device operates in reflection mode and consists of a short segment of photonic crystal fiber (PCF) inserted in conventional single-mode optical fiber (SMF). A microscopic collapsed zone in the PCF–SMF junction allows the excitation and recombination of core modes, hence, to build a mode interferometer. Bending on the device induces asymmetric refractive index changes in the PCF core as well as losses. As a result, the effective indices and intensities of the interfering modes are altered, which makes the interference pattern shift and shrink. The asymmetric index changes in the PCF make our device capable of distinguishing the bending orientation. The sensitivity of our sensor is up to 1225 pm/degree and it can be used to monitor small bending angles (±2°). We believe that the attributes of our sensor make it appealing in a number of applications.

OCIS codes: (060.2370) Fiber optics sensors; (060.5295) Photonic crystal fibers; (060.4005) Microstructured fibers; (280.4788) Optical sensing and sensors; (120.3180) Interferometry.

http://dx.doi.org/10.1364/OL.40.003113

Bending (tilt or inclination) sensors have important applications in civil engineering as they can be used for monitoring the verticality of buildings, towers, bridge piles, and many other infrastructures. For these applications, sensors that are highly sensitive and that can resolve small bending angles are highly desirable. Additional features of bending sensors include compactness, simplicity, accuracy, reliability, etc. To achieve such features, the optical fiber sensor community has proposed a number of sensing architectures. Most of them are based on Bragg gratings [1–5], long-period gratings (LPGs) [6–12], interferometers [13–19], or on intensity measurements involving optical fibers [20–23].

The majority of fiber optic bending sensors has important limitations. For example, those based on Bragg gratings exhibit low sensitivity for small angles, typically require additional reference sensors, and are not capable of distinguishing the orientation of the bending [1–5]. On the other hand, the performance of LPG-based bending sensors can be compromised by surrounding or packaging materials as LPGs are sensitive to the medium that envelops the optical fiber [6–12]. The disadvantage of some interferometric bending sensors is their complexity as they require several components that must be precisely aligned [16]. On the other hand, bending sensors based on intensity measurements require a mechanism to compensate fluctuations of the light source or attenuation losses [20–23].

Bending sensors based on specialty optical fibers, such as multicore fibers (MCFs) [1,18] or photonic crystal fibers (PCFs) [14,15,17], partially overcome the aforementioned disadvantages. However, the bending sensitivities of MCF sensors [18] are low for small angles, while the fabrication of some PCF bending sensors involves a manual process that typically leads to low reproducibility [14,17].

Here, we report on a PCF mode interferometer that exhibits high bending angle sensitivity (up to 1225 pm/degree), can operate in a small angle region (±2°), and can distinguish the orientation of the bending. In addition, its fabrication is carried out with well-established fiber optic instrumentation, and its interrogation is simple as light sources and detectors used for telecommunications or to interrogate fiber Bragg grating sensors can be used. We believe that the sensing configuration proposed here overcomes the main limitations of the majority of fiber optic bending sensors.

Figure 1 shows a drawing of our PCF mode interferometer [24,25], a schematic representation of its interrogation, the cross section of the PCF used in the experiments, the modes that participate in the interference, and a micrograph of the PCF–SMF splice. Basically, the device consists of a short segment of homemade PCF inserted at the end of a conventional single-mode optical fiber (SMF) (Corning SMF-28). To do so, we joined both fibers with an inexpensive fusion splicing machine (Ericsson FSU-975). An *ad hoc* splicing program was

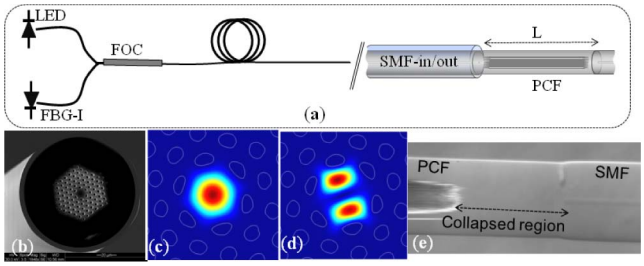

Fig. 1. (a) Schematic representation of the PCF interferometer whose interrogation comprises a light-emitting diode (LED), a fiber optic coupler (FOC), and a fiber Bragg grating interrogator (FBG-I). L is the length of PCF. (b) Microscopic image of the cross section of the PCF used in the experiments. Images (c) and (d) show the fundamental and second-order modes of the PCF that participate in the interference and (e) is a micrograph of the PCF–SMF junction. Figures (b)–(d) were taken from Ref. [25].

developed so that the voids of the PCF collapsed in a microscopic region whose length was ~175 μm in all cases [see Fig. 1(e)]. As the PCF and SMF had similar outer diameters (125 μm), the splicing was carried out in automatic mode. The splicing process makes the PCF and SMF permanently aligned, therefore, the device is axially symmetric.

The working mechanism of our interferometer has been discussed in detail in [24,25]. Basically, in the collapsed zones of the PCF, the propagating beam broadens due to diffraction. As a consequence, there is a mode field mismatch between the PCF and SMF. The latter combined with the axial symmetry and modal properties of the PCF is what allows the excitation (and recombination) of azimuthally symmetric modes [25] [see Figs. 1(c) and 1(d)]. As the modes excited in the PCF have different effective indices, they travel at different speeds. Thus, they accumulate a phase difference as they propagate along the length of the PCF. The phase difference will depend on the length of the PCF and also on the wavelength of the light source. Thus, the reflected spectrum of our interferometer is expected to exhibit periodic maxima and minima (see Fig. 2).

The reflection of our device can be expressed as

$$I_R = I_1 + I_2 + 2(I_1 \cdot I_2)^{1/2} \cos(2\pi \Delta n L/\lambda). \quad (1)$$

In Eq. (1), I_1 and I_2 are the intensities of the interfering modes, Δn is the difference between the effective indices of the interfering modes, L is the length of the PCF, and λ is the wavelength of the light source. Maxima of Eq. (1) appear when $2\pi \Delta n L/\lambda = 2m\pi$, $m = 1, 2, 3\ldots$ This means that I_R will exhibit maxima at wavelengths that satisfy the following expression:

$$\lambda_m = \Delta n L/m. \quad (2)$$

To investigate the performance of our interferometer as a bending sensor, we implemented two simple setups. One of them is shown in Fig. 2, in which a long interferometer ($L = 37$ mm) was placed in pendulum position. The interferometer was immobilized with a fiber rotator (HFR007, Thorlabs). The collapsed region of the PCF was at the edge of the rotator as illustrated in Fig. 2. A 100 g fiber chuck was used as a weight, which

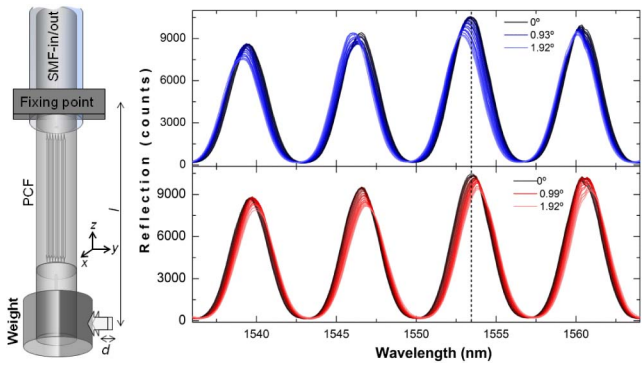

Fig. 2. Schematic representation of the pendulum-type configuration used to bend the interferometer. l is the distance from the fixing point to the point where the device is bent and d is the displacement of the weight. The graphs show the reflection spectra observed when the device was bent in the 0°–1.92° range in steps of 0.055°. The top graph shows the spectra observed when the bending was in the $-y$ direction and the bottom graph shows those when the bending was in the $+y$ direction. L was 37 mm in all cases.

was sufficient to keep the interferometer straight. The interference pattern observed in the direction of gravity was taken as reference. In this reference position, the stability over time of the interferometer was studied. The results are summarized in Fig. 3. It can be noted that the shift of the interference pattern is less than ±10 pm; such a shift is within the range that our FBG interrogator (I-MON-512 USB, IBSEN Photonics) could resolve. The results shown in Fig. 3 demonstrate that our interferometer is highly stable over time, which is important for reliable measurements.

Bending to the interferometer in $-y$ and $+y$ directions (see Fig. 2) were introduced with precise micropositioners (3-Axis NanoMax Stage, Thorlabs). The distance between the fixing point of the device and the point of the translation stage that displaced the mass (l) was 50.45 mm. The maximum displacement (d) of the mass was ±1.80 mm. The results of the experiments are shown in Fig. 2. A shift to a shorter wavelength (blue shift) was observed when the interferometer was bent in the $-y$

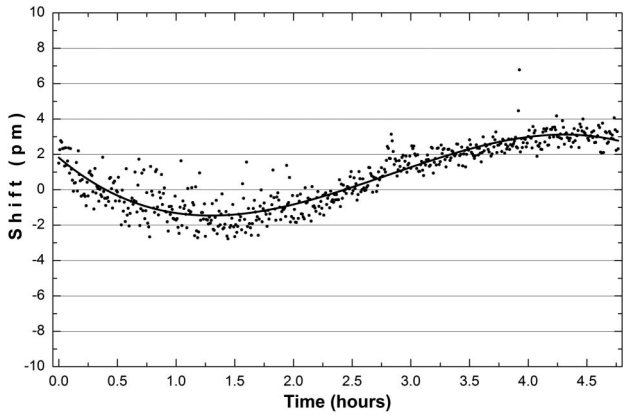

Fig. 3. Shift of the interference pattern as a function of time observed in a 37 mm long interferometer when it was in pendulum position and no bending was induced. The interference pattern was monitored in the 1510–1590 nm range.

direction and a shift to longer wavelengths (red shift) was observed when the device was bent in the $+y$ direction. It can also be observed that regardless of the orientation of the bending, the interference patterns shrink slightly.

The performance of our interferometer as a bending sensor was also investigated in a cantilever-like position (see Fig. 4). In this case, a short interferometer ($L = 17.3$ mm) was used. The interferometer was also immobilized with a fiber rotator and the collapsed region of the PCF was at the edge of the rotator as illustrated in Fig. 4. The free extremity of our device had a cleaved end that acted as a low-reflectivity mirror. Bending was also introduced with the precise micropositioners mentioned above. Figure 4 shows the spectra observed when the interferometer was bent in the $-y$ direction (blue shift) and $+y$ direction (red shift). It can be observed that the shift of the interference pattern and the changes of intensity are more prominent than those achieved in pendulum position with a longer device.

The shifts observed in the interference patterns as a function of bending angle for the two configurations mentioned above are shown in Fig. 5. The behavior of our interferometer is linear in the two bending configurations studied. The bending sensitivities of the 37 mm long interferometer were found to be −238 and +202 pm/degree for the $-y$ and $+y$ directions, respectively. The corresponding sensitivities for the 17.3 mm long interferometer were found to be −1270 and +1174 pm/degree, respectively. As a shift of ∼20 pm can be resolved, the resolution of our short device is ∼0.015°. We would like to point out that other vector fiber optic bending sensors reported in the literature also exhibit sensitivities that depend on the bending direction, but they are more complex and their resolutions are lower [3,10,17].

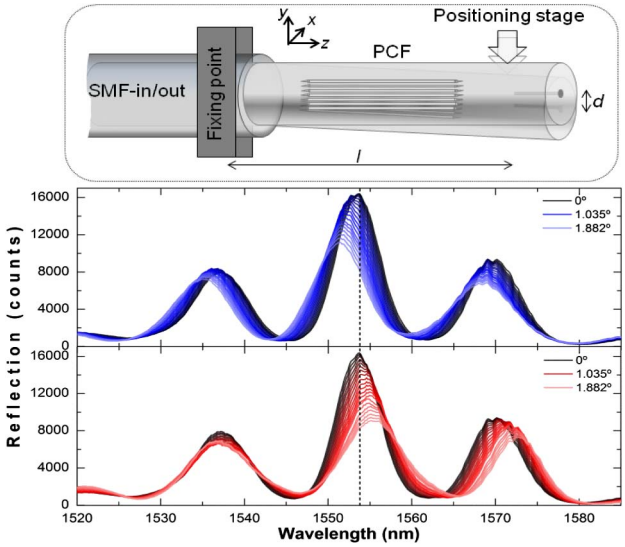

Fig. 4. Schematic representation of the cantilever-type configuration used to bend the interferometer. The graphs show the reflection spectra observed in the 0°–1.88° range in steps of 0.094°. The blue shift was observed when the direction of the bending was in the $-y$ direction (top graph) and the red shift was when the direction of the bending was in the $+y$ direction (bottom graph). L was 17.3 mm in all cases.

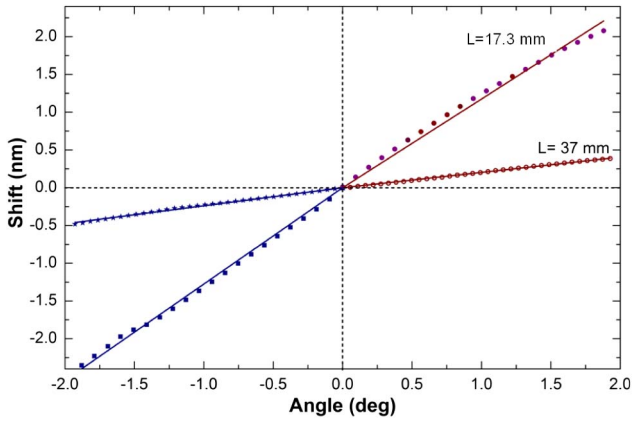

Fig. 5. Shift of the interference pattern as a function of bending angle observed in two devices with different lengths. Negative angles are when the device is bent in the $-y$ direction, according to the coordinate systems shown in Figs. 2 and 4.

The behavior of our interferometer can be explained as follows: when the PCF is bent, a small geometrical deformation is introduced in the axis of the fiber as well as minute changes in the refractive index of the PCF core [26,27]. As a consequence, the effective indices of the interfering modes are altered; hence, Δn changes and the interference pattern shifts. This means that according to Eq. (2), the position of λ_m changes. As a shift of the interference pattern can be monitored with high accuracy, a high bending sensitivity can be expected. The visibility (fringe contrast) of an interference pattern depends on the intensities of the interfering modes (I_1 and I_2), which change when the PCF is bent [26–28]. As a result, the interference pattern shrinks when the device is subjected to bending. The high sensitivity observed in the shorter device is due to the higher refractive index changes that occur when $l(R)$ is small.

The sensitivity to the bending orientation can be explained as follows: the refractive index of an optical fiber (here our PCF) changes when it is bent [26–28]. The refractive index distribution of the core of the bent fiber is gradual and can be expressed as [26]

$$n \approx n_0 + n_0 y/R, \tag{3}$$

where n_0 is the index of the fiber core when it is straight and R is the radius of curvature, which can be related with the bending angle as [16] $R \approx l^2/(2d)$, where l and d are described in Figs. 2 and 4. The y axis is also shown in Figs. 2 and 4. The above expression is valid for n when $y = 0$ is in the geometrical center of the optical fiber.

From Eq. (3) it is clear that bending of the PCF in the $+y$ direction will increase the refractive index of the fiber core, and consequently, the effective indices of the interfering modes; hence, Δn will increase. Thus, according to Eq. (2), if Δn augments, then λ_m will increase, which means the interference pattern will shift to longer wavelengths (a red shift). When bending is in the $-y$ direction, the opposite effect can be expected, which means Δn will decrease, and consequently, λ_m will decrease, which will result in a blue shift of the interference pattern. A more detailed analysis of this effect is discussed in Refs. [17,27,28]. In those works, it was also demonstrated that

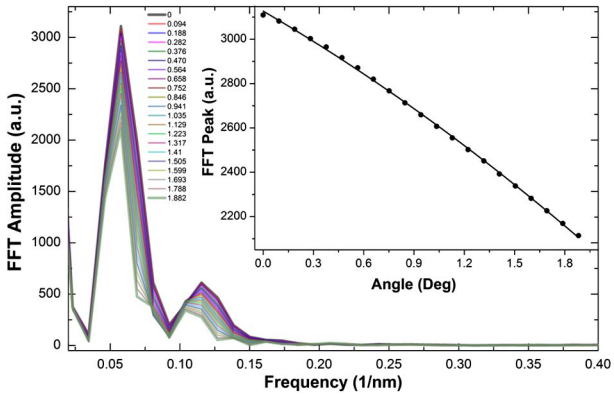

Fig. 6. Amplitude of the FFT as a function of frequency for bending angles in the 0°–1.882° range. The inset shows the value of the highest peak of the FFT as a function of bending angle. Bending was carried out in a cantilever configuration and $L = 17$ mm.

bending also induces asymmetry in the intensity distributions of the interfering modes because the intensity is higher in the zones of higher refractive index. This means that bending breaks the symmetry of the higher order mode shown in Fig. 1(d).

The changes in the visibility (or fringe contrast) of the interference pattern can also be used to quantify the bending on the fiber [29,30]. However, this approach is not convenient in a situation of high attenuation losses, introduced, e.g., by connectors, where the minima of the interference pattern can approach the floor noise of the detector or spectrum analyzer. Here, instead, we propose to quantify the bending on the interferometer by monitoring the amplitude of the fast Fourier transform (FFT) of the interference patterns. Such a method is simple and as the FFT does not depend on Δn or L but on the changes of the intensities of the interfering modes, it is independent of temperature as demonstrated in [30].

Figure 6 shows the FFT amplitude as a function of frequency for bending angles between 0 and 1.88°. The figure also shows the peak value of the fundamental frequency (FF) of the FFT as a function of the bending angle (inset). The FF (the highest peak) is located at $1/P$, where P is the period of the interference pattern. The results shown in the figure were calculated with the spectra shown Fig. 4 when the bending was in the $+y$ direction.

In conclusion, here we have reported on a compellingly simple vector bending sensor based on a PCF mode interferometer. Bending on the PCF induces a dual effect on the interfering modes, refractive index changes, and losses. Such a dual effect causes a shift and changes the visibility to the interference pattern. To monitor visibility changes, we used Fourier transformation as this is not affected by power fluctuations of the light source or temperature changes. Our device exhibits high sensitivity (up to 1270 pm/degree), can operate in a small angle region (±2°), and can distinguish the direction of the bending angle. We believe that the simplicity and flexibility of our device make it attractive for practical applications.

Funding. FEDER funds; Gobierno Vasco/Eusko Jaurlaritza (IT664-13, ETORTEK14/13); IKERBASQUE; Ministerio de Economía y Competitividad (Spain) (TEC2012-37983-C03-01); University of the Basque Country (UPV/EHU) (UFI11/16US13/09, EUSKAMPUS)

REFERENCES

1. M. J. Gander, W. N. Macpherson, R. McBride, J. D. C. Jones, L. Zhang, I. Bennion, P. M. Blanchard, J. G. Burnett, and A. H. Greenaway, Electron. Lett. **36**, 120 (2000).
2. X. Dong, Y. Liu, Z. Liu, and X. Dong, Opt. Commun. **192**, 213 (2001).
3. L.-Y. Shao and J. Albert, Opt. Lett. **35**, 1034 (2010).
4. A. Rauf, J. Zhao, B. Jiang, Y. Jiang, and W. Jiang, Opt. Lett. **38**, 214 (2013).
5. D. Barrera, I. Gasulla, and S. Sales, J. Lightwave Technol. **33**, 2445 (2015)
6. H. J. Patrick, C. C. Chang, and S. T. Vohra, Electron. Lett. **34**, 1773 (1998).
7. C. C. Ye, S. W. James, and R. P. Tatam, Opt. Lett. **25**, 1007 (2000).
8. Y. P. Wang and Y. J. Rao, IEEE Sens. J. **5**, 839 (2005).
9. L.-Y. Shao, A. Laronche, M. Smietana, P. Mikulic, W. J. Bock, and J. Albert, Opt. Commun. **283**, 2690 (2010).
10. P. Saffari, T. Allsop, A. Adebayo, D. Webb, R. Haynes, and M. M. Roth, Opt. Lett. **39**, 3508 (2014).
11. A. Taghipour, A. Rostami, M. Bahrami, H. Baghban, and M. Dolatyari, Opt. Commun. **312**, 99 (2014).
12. Q. Zhou, W. Zhang, L. Chen, Z. Bai, L. Zhang, L. Wang, B. Wang, and T. Yan, IEEE Photon. Technol. Lett. **27**, 713 (2015).
13. D. Inaudi and B. Glisic, Proc. SPIE **4694**, 36 (2002).
14. Z. L. Ou, Y. Yu, P. Yan, J. Wang, Q. Huang, X. Chen, C. Du, and H. Wei, Opt. Express **21**, 23812 (2013).
15. H. Gong, H. Song, X. Li, J. Wang, and X. Dong, Sens. Actuators A **195**, 139 (2013).
16. H. Qu, G. F. Yan, and M. Skorobogatiy, Opt. Lett. **39**, 4835 (2014).
17. Q. Huang, Y. Yu, X. Li, X. Chen, Y. Zhang, W. Zhou, and C. Du, Opt. Express **23**, 3010 (2015).
18. G. Salceda, A. Van Newkirk, J. Antonio-Lopez, A. Martínez-Rios, A. Schulzgen, and R. Amezcua, Opt. Lett. **40**, 1468 (2015).
19. L. Zhang, W. Zhang, L. Chen, T. Yan, L. Wang, B. Wang, and Q. Zhou, IEEE Photon. Technol. Lett. **27**, 1240 (2015).
20. K. S. C. Kuang, W. J. Cantwell, and P. J. Scully, Meas. Sci. Technol. **13**, 1523 (2002).
21. A. Khiat, F. Lamarque, C. Prelle, N. Bencheikh, and E. Dupont, Meas. Sci. Technol. **21**, 025306 (2010).
22. Y. G. Lee, H. K. Jang, D. H. Kim, and C. G. Kim, Sens. Actuators A **184**, 46 (2012).
23. H. Qu, T. Brastaviceanu, F. Bergeron, J. Olesik, I. Pavlov, T. Ishigure, and M. Skorobogatiy, Appl. Opt. **52**, 6344 (2013).
24. J. Villatoro, V. Finazzi, V. P. Minkovich, V. Pruneri, and G. Badenes, Appl. Phys. Lett. **91**, 091109 (2007).
25. G. Coviello, V. Finazzi, J. Villatoro, and V. Pruneri, Opt. Express **17**, 21551 (2009).
26. K. Nagano, S. Kawakami, and S. Nishida, Appl. Opt. **17**, 2080 (1978).
27. J. C. Baggett, T. M. Monro, K. Furusawa, V. Finazzi, and D. J. Richardson, Opt. Commun. **227**, 317 (2003).
28. N. Hai Vu, I.-K. Hwang, and Y.-H. Lee, Opt. Lett. **33**, 119 (2008).
29. O. Frazão, R. Falate, J. L. Fabris, J. L. Santos, L. A. Ferreira, and F. M. Araújo, Opt. Lett. **31**, 2960 (2006).
30. J. Villatoro, V. P. Minkovich, and J. Zubia, IEEE Photon. Technol. Lett. **27**, 1181 (2015).